Dipolar resonances in conductive carbon micro-fibers probed by near-field terahertz spectroscopy

I. Khromova,[1,2,3] M. Navarro-Cía,[1,4] I. Brener,[5,6] J. L. Reno,[5,6] A. Ponomarev,[7] and O. Mitrofanov[1,5]

[1)] *Department of Electronic and Electrical Engineering, University College London, Torrington Place, London WC1E 7JE, United Kingdom*

[2)] *International Research Centre for Nanophotonics and Metamaterials, ITMO University, Birjevaja line V.O. 14, St. Petersburg 199034, Russia*

[3)] *Department of Electrical and Electronic Engineering, Public University of Navarra, Arrosadia, Pamplona, Navarra 31006, Spain*

[4)] *Optical and Semiconductor Devices Group, Department of Electrical and Electronic Engineering, Imperial College London, SW7 2BT, London, UK*

[5)] *Center for Integrated Nanotechnologies, Sandia National Laboratory, Albuquerque, MN 87185, USA*

[6)] *Sandia National Laboratory, Albuquerque, MN 87185, USA*

[7)] *St. Petersburg State Polytechnic University, Politekhnicheskaya 29K1, St. Petersburg 194064, Russia*

(Dated: 14 July 2015)

We observe dipole resonances in thin conductive carbon micro-fibers by detecting an enhanced electric field in the near-field of a single fiber at terahertz (THz) frequencies. Time-domain analysis of the electric field shows that each fiber sustains resonant current oscillations at the frequency defined by the fiber's length. Strong dependence of the observed resonance frequency and degree of field enhancement on the fibers' conductive properties enable direct non-contact probing of the THz conductivity in single carbon micro-fibers. We find the conductivity of the fibers to be within the range of 1-5 $\times 10^4$ S/m. This approach is suitable for experimental characterization of individual doped semiconductor resonators for THz metamaterials and devices.

Resonant plasmonic response of micro-scale structures made of doped semiconductors at terahertz (THz) frequencies enables tunable light-matter interaction required for efficient THz devices. A semiconductor micro-resonator, for instance, can be used as a tunable antenna for THz sensing and detection[1–3]. Arranged in a periodic array, such antennas offer promising solutions for tunable THz metamaterials with frequency-selective transmition and absorption[4–7].

At the heart of the tunable THz response is the dependence of the resonance properties of semiconductor micro-structures on their plasma frequency and charge carrier scattering rate. These parameters are tunable via electronic, thermal and chemical mechanisms within the THz and mid-IR frequency ranges. They are also influenced by fabrication processes and handling conditions. Experimental methods for THz conductivity characterization are therefore required for verifying theoretical models of semiconductor micro-structures (including periodic arrays of graphene ribbons or randomly disributed carbon nanotubes and micro-fibers) and for the development of tunable THz devices.

The two most common experimental techniques for characterizing nano- and micro-particles at THz frequencies rely on models of their collective response. The first approach consists in measuring THz transmission or reflection in composites containing multiple resonators[8–10]. Extracting the properties of individual resonators from such measurements requires knowledge of their shape, dimensions, volume fraction, and degree of clusterization. It is common to use effective media approximations, such as the Maxwell-Garnett mixing rule, to describe composites with subwavelength inclusions[11]. However, this approach is not applicable to composites with inhomogeneous, resonant or irregularily shaped inclusions[11,12], in particular those with sizes comparable to the relevant wavelength. In the second approach, micro-resonators are analyzed by measuring THz transmission or reflection of metasurfaces containing their periodic or a-periodic arrays[1,3]. However, the collective response of a metasurface is defined by both the response of individual elements and the interaction between them. Moreover, each of the resonant elements may have different conductivity or size giving rise to a broader collective resonance. Local carrier density in semiconductors has been probed using tip-enhanced spectroscopy in the THz and infrared ranges[13,14]. Observation and characterization of plasmonics excitations using this method for individual THz resonators have not been reported yet. It is thus important to have a technique for direct experimental characterization of single resonant micro-particles at THz frequencies.

In this letter, we report on an experimental method for non-contact probing of THz conductivity in individual conductive micro-resonators. We studied single carbon micro-fibers (CMFs), with lengths varying between 50 and 150 μm, using near-field time-domain THz spectroscopy[15,16]. For each fiber, we observe an electric dipole resonance in the THz range. At the resonance frequency, specific for each CMF, the electric field in the near-field zone of the fiber is enhanced. Time-domain analysis allows us to attribute the enhancement to standing waves, or plasmonic resonances, induced in the CMFs by incident THz pulses. The degree of field enhancement,

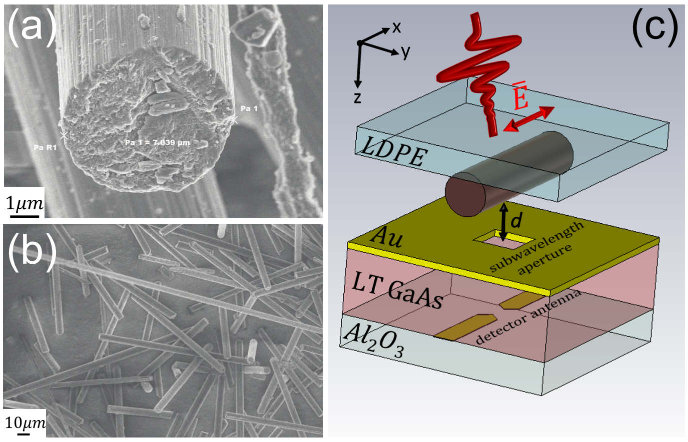

FIG. 1. (a,b) Scanning electron microscope images of CMFs. (c) Sketch of the the THz near-field time-domain spectroscopy setup (not to scale).

as well as the resonance frequency, for a conductive fiber depend primarily on the material's DC conductivity. It allows us to experimentally evaluate the conductivity of a single CMF through studying the properties of its resonant response. To do so, we compare the measured resonance frequency and enhancement factor with those computed using full-wave numerical modelling. The THz conductivity of the CMFs is similar to that of doped semiconductors, suggesting that the method can be applied to a broad range of THz plasmonic resonators.

A CMF (Fig. 1(a,b)) is a cylindrical particle with a 7 μm diameter and a length of the order of tens of μm, produced from carbon fibers by micro-milling (supplied by STC of Applied Nanotechnologies). It contains 98% carbon basis and its crystal structure resembles that of graphite with sheets oriented along the fiber axis[17,18]. Depending on specific fabrication techniques, the DC resistivity of similar unmilled carbon fibers is of the order of 10 $\mu\Omega\times$m[17] and is strongly temperature-dependent[19]. The plasma frequency of graphite in the conductive plane is within the range of 0.17-0.83 eV[20,21], which is significantly above the THz region and corresponds to carrier density of order of 10^{18} cm^{-3}.

In our experimental method, a single CMF is exposed to a broadband THz pulse and the sample's response is detected in the fiber's near-field zone through a subwavelength square aperture (10×10 μm^2) in a metallic screen. In the vicinity of the CMF dipole, resonant currents induce quasi-static enhanced fields oscillating at the frequency determined by the fiber's length[22,23]. The field couples through the subwavelength aperture allowing the photocoductive THz detector[15] to record the resonant response. This technique was recently used to study THz Mie resonances in dielectric micro-spheres[24]. The incident pulse spectrum in our experiment (0.5-2.5 THz) covers the fundamental dipole resonances for CMFs with lengths ranging from $\approx$ 50 to $\approx$ 300 μm, which is roughly equal to $\lambda/2$ (half-wavelength in free space).

Although the proximity of the samples to the metallic screen of the probe surface introduces a ground plane effect, known to deteriorate the radiative efficiency of dipoles[22], the near-field response of CMFs nevertheless remains resonant. In the frequency domain, the spectrum of the detected field produces a pronounced peak at the resonance frequency specific to each CMF.

CMF samples are manually attached to 12.5 μm-thick low-density polyethylene (LDPE) substrates. The fiber axis is oriented along the polarization (x-axis) of the THz pulses generated by optical rectification in a ZnTe crystal. The experiments are performed at a temperature of $22^\circ\pm1^\circ$C.

Figure 2(a) shows the near-field space-time distribution (200 μm$\times$12 ps) of the electric field detected by the THz probe along the axis of a 80 μm-long CMF. Figures 2(b,c) illustrate the waveforms detected by the probe with and without the fiber in front of the probe aperture, respectively. These measurements are taken at the same sample-to-proble distance, $d=15$ μm. Throughout the experiment, d is kept below $\lambda/6$ (λ is the central free-space wavelength) ensuring near-field measurements.

The space-time diagrams and waveforms measured at the centers of all CMFs show clear resonant features - each sample is 'ringing' at a specific frequency. This fact allows us to create time-resolved THz images of CMF resonant modes by raster scanning the fiber in the xy-plane while maintaining the same sample-to-probe distance. The THz image in Fig. 2(d) is recorded at 3.5 ps time delay, when the field of the resonant standing wave is at its maximum and is distinctly different from the field detected in the absence of the sample. The detected field is proportional to the gradient $\frac{dE_z}{dx}$ of the field induced between the CMF and the ground plane[25](see inset in Fig. 2(e)). Figure 2(e) shows the spectral response of the CMF with the resonance peak matching the THz dipole resonance. In the vicinity of the resonant frequency, the spectrum follows a Lorentzian line shape and can be described by two parameters: the resonance frequency f_r and the peak amplitude (normalized to the reference spectrum, $E(f_r)/E_0(f_r)$). For simplicity, let us denominate the latter as the enhancement factor (EF).

Our approach to finding the CMF's conductivity is through measuring its EF. Similar to its effect on scattering and absorption cross-sections of a dipole in the far field, the dipole's conductivity defines the intensity of induced resonant currents and, consequently, the strength of the fields in the immediate proximity to the CMF.

The observed response of a micro-resonator with a certain conductivity also depends on its distance from the metallic screen of the probe. As the sample is moved towards the probe along the z-axis, the detected near-feld amplitude increases and produces higher enhancement factor EF[26]. For each sample, we measure the dependence of its EF on the sample-to-probe distance d.

Figure 3(a,b) show the enhancement factor vs. distance diagrams for a 102 μm and 80 μm-long CMFs, respectively. The black lines and symbols denote the

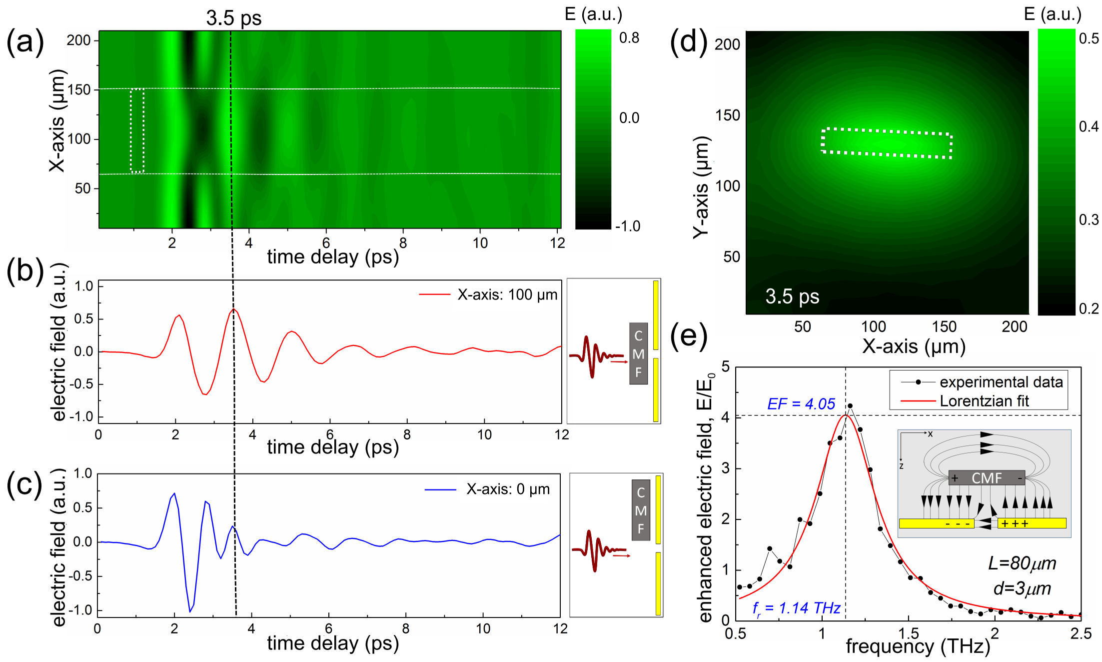

FIG. 2. (a) The space-time diagram showing the change in the detected waveform as the probe scans along a 80 μm CMF placed at a distance of $d = 15$ μm away from the probe. (b), (c) Waveforms detected in front of (red) and away from (blue) the CMF. Schematic images depict the positions of the sample with respect to the aperture. (d) THz near-field image of the detected field distribution around the CMF (outlined schematically), taken at a fixed time delay of 3.5 ps. The spatial resolution is defined by the aperture size and is 10 μm. (e) Spectrum and its Lorentzian fit of the same CMF placed at $d = 3$ μm (normalized to reference spectrum), inset: schematic diagram of the electric field distribution at the CMF resonance.

measured enhancement factors for both CMFs, the blue lines and symbols represent the corresponding enhancement factors extracted from the Lorentzian fits to the measured spectra, as in Fig. 2(e).

To evaluate the CMF's conductivity, we simulate the experiment (including the sample, the substrate and the probe) numerically using the time-domain solver of the CST Microwave Studio^{TM}. We use hexahedral mesh cells with sizes varying from 0.1 to 10 μm. The CMF's conductivity at THz frequencies is approximated by a DC value and is varied from 10^3 to 10^8 S/m. Losses in the LDPE substrate are neglected.

In Fig. 3(a,b), the experimental curves are plotted against numerically obtained conductivity maps. As the sample-to-probe distance increases, the influence of systematic noise becomes more noticeable, which can be seen from the error bars. Comparing the results, we conclude that the DC conductivity of the CMFs is within 1-5$\times 10^4$ S/m, which is consistent with estimations based on conductive properties of graphite[21].

An alternative, and probably more intuitive, approach to estimating the conductivity of lossy dipoles consists in measuring their resonance frequency. As the conductivity decreases and the material's response deviates from perfect electric conductor, the period of resonant current oscillations becomes longer and the resonance frequency of the dipole shifts towards lower values.

Compared to the case of suspended dipole, in our experiment, the resonance for each CMF experiences an additional 'red' frequency shift and almost a double increase of the enhancement factor. This is due to the presence of LDPE substrates with a dielectric permittivity $\epsilon_{sub} = 2.33$ [27]. For perfect conductors, the resonance frequency shift can be estimated as a factor of $\sqrt{\frac{2}{\epsilon_{sub}+1}}$.

In addition to the effect of the LDPE substrates, the resonance frequency of each dipole is also affected by the metallic plane of the probe[22]. Figure 3(c) shows a resonance frequency vs. sample-to-probe distance diagram similar to Fig. 3(a,b) with experimental data plotted against the numerically obtained conductivity map for a 80 μm CMF. The conductivity of the CMFs measured via this approach is consistent with the one estimated through enhancement factor analysis.

In these experiments the following factors affect the accuracy of conductivity estimation. The lengths of the studied CMFs were measured with about ± 1 μm error, which would change the EF and the resonance frequency by $\sim 1\%$. CMF radii were not measured for each individual sample, but assumed to be equal to 3.5 μm as in Fig. 1(a). It is known that the radii of the CMFs experience a 10% variation resulting in 10% and $< 1\%$ error in the EF and f_r, respectively. The distance between the sample and the detector d was defined with a ± 2 μm error. More precise definition of d can further improve the accuracy of the conductivity measurements.

In conclusion, we present an experimental method for

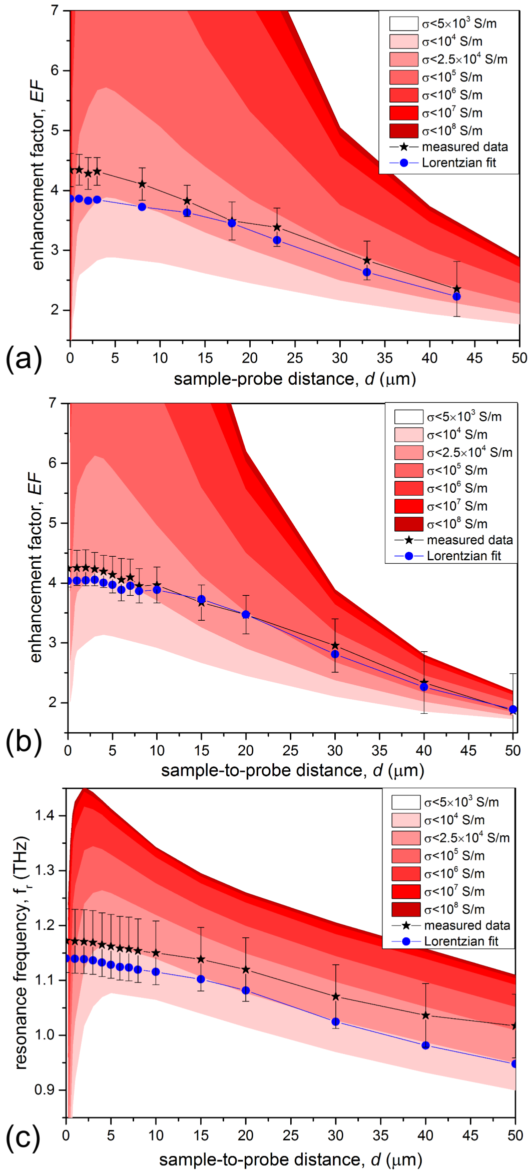

FIG. 3. (a),(b) Enhancement factor EF vs. distance between the sample and the probe for CMFs with lengths $L = 102$ μm and $L = 80$ μm, respectively. (c) Resonance frequency f_r vs. distance between the sample and the probe for $L = 80$ μm. Coloured zones mark numerically calculated areas corresponding to different conductivity bands within the range of 10^3-10^8 S/m. Black curves and symbols represent the measured EF and f_r, while blue curves and symbols correspond to EF and f_r extracted from Lorentzian fitted experimental spectra. The error bars depict the measurement errors related to (a), (b) noise and (c) spectral resolution of 58 GHz.

non-contact probing of the THz conductivity of single, conductive resonant micro-particles. As a proof of concept, we measured the THz conductivity of individual CMFs by 1) measuring the degree of near-field enhancement produced by the electric dipole resonances in the near-field region around the samples, 2) and analyzing their resonance frequency and its deviation from the resonance frequency of perfectly conducting dipoles with identical geometry. The difference in the way experimental errors affect the two measured parametres, EF and f_r, suggests that the two techniques of conductivity estimation are complementary to each other. We note that far-field characterization of isolated resonant microstructures using a conventional THz time-domain spectroscopy (TDS) system is challenging. With their typical beam spot size of $\approx$ 1mm in diameter, an 80 μm CMF (assuming its conductivity to be 2.5×10^4 S/m) would lead to a mere 1.7% intensity dip (0.88% amplitude dip) in transmitted field. The proposed near-field approach is suitable for characterizing isolated micro-scale particles with pronounced resonant absorption in the THz range and works best for materials with low DC conductivity (10^3-10^6 S/m). In particular, it can be applied to characterization of semiconductor or semimetallic elements of THz absorbers, resonance-based sensors or tunable metamaterials and metasurfaces.

This work is supported by the Royal Society [Grant No. UF130493], RFBR [Project No. 14-22-02064 ofi-m] and Imperial College London [Junior Research Fellowship] and partially supported by the Government of the Russian Federation [Grant No. 074-U01]. This work was performed at UCL and, in part, at the Center for Integrated Nanotechnologies, a U.S. Department of Energy, Office of Basic Energy Sciences user facility. Sandia National Laboratories is a multi-program laboratory managed and operated by Sandia Corporation, a wholly owned subsidiary of Lockheed Martin Corporation, for the U.S. Department of Energy's National Nuclear Security Administration under contract DE-AC04-94AL85000. The authors thank FideNa (Spain) for the SEM images.

[1] A. Berrier, P. Albella, M. A. Poyli, R. Ulbricht, M. Bonn, J. Aizpurua, and J. G. Rivas, Opt. Express **20**, 5052 (2012).
[2] G. Georgiou, A. Berrier, M. Schaafsma, H. Tyagi, M. Nagel, and J. Gomez Rivas, in *38th International Conference on Infrared, Millimeter, and Terahertz Waves (IRMMW-THz)* (2013) pp. 1–3.
[3] B. Ng, S. M. Hanham, V. Giannini, Z. C. Chen, M. Tang, Y. F. Liew, N. Klein, M. H. Hong, and S. A. Maier, Opt. Express **19**, 14653 (2011).
[4] L. Ju, B. Geng, J. Horng, C. Girit, M. Martin, Z. Hao, H. A. Bechtel, X. Liang, A. Zettl, Y. R. Shen, and F. Wang, Nat. Nano. **6**, 630 (2011).
[5] J. Han, A. Lakhtakia, and C.-W. Qiu, Opt. Express **16**, 14390 (2008).
[6] H.-T. Chen, Front. Optoelectron. **8**, 27 (2015).
[7] D. R. Chowdhury, R. Singh, J. F. O'Hara, H.-T. Chen, A. J. Taylor, and A. K. Azad, Appl. Phys. Lett. **99**, 231101 (2011).
[8] J. Lloyd-Hughes and T.-I. Jeon, J. of Infrared Millim. THz Waves **33**, 871 (2012).
[9] H. J. Joyce, C. J. Docherty, Q. Gao, H. H. Tan, C. Jagadish, J. Lloyd-Hughes, L. M. Herz, and M. B. Johnston, Nanotechnology **24**, 214006 (2013).
[10] A. Mazhorova, J. F. Gu, A. Dupuis, M. Peccianti, O. Tsuneyuki, R. Morandotti, H. Minamide, M. Tang, Y. Wang, H. Ito, and M. Skorobogatiy, Opt. Express **18**, 24632 (2010).
[11] A. Sihvola, *Electromagnetic Mixing Formulas and Applications*,

IEEE Electromagnetic Waves Series (Institution of Electrical Engineers, 1999).
[12] P. Kužel and H. Němec, J. Phys. D: Appl. Phys. **47**, 374005 (2014).
[13] A. J. Huber, F. Keilmann, J. Wittborn, J. Aizpurua, and R. Hillenbrand, *Nano Letters*, Nano Lett. **8**, 3766 (2008).
[14] M. C. T. L. Eisele, M. A. Huber, M. Plankl, L. Viti, D. Ercolani, L. Sorba, M. S. Vitiello, and R. Huber, Nat Photon **8**, 841 (2014).
[15] A. J. Macfaden, J. L. Reno, I. Brener, and O. Mitrofanov, Appl. Phys. Lett. **104**, 011110 (2014).
[16] J. R. Knab, A. J. L. Adam, E. Shaner, H. J. A. J. Starmans, and P. C. M. Planken, Opt. Express **21**, 1101 (2013).
[17] D. D. Chung, *Carbon Fiber Composites*, tagkey1994iii (Butterworth-Heinemann, Boston, 1994).
[18] X. Huang, Materials **2**, 2369 (2009).
[19] I. L. Spain, K. J. Volin, H. A. Goldberg, and I. L. Kalnin, Solid State Communications **45**, 817 (1983).
[20] L. G. Johnson and G. Dresselhaus, Phys. Rev. B **7**, 2275 (1973).
[21] R. C. Tatar and S. Rabii, Phys. Rev. B **25**, 4126 (1982).
[22] S. Schelkunoff and H. Friis, *Antennas: theory and practice*, Applied mathematics series (Wiley, 1952).
[23] E. S. Barnard, J. S. White, A. Chandran, and M. L. Brongersma, Opt. Express **16**, 16529 (2008).
[24] O. Mitrofanov, F. Dominec, P. Kužel, J. L. Reno, I. Brener, U.-C. Chung, C. Elissalde, M. Maglione, and P. Mounaix, Opt. Express **22**, 23034 (2014).
[25] R. Mueckstein, C. Graham, C. C. Renaud, A. J. Seeds, J. A. Harrington, and O. Mitrofanov, J. Infrared Millim. Terahertz Waves **32**, 1031 (2011).
[26] M. Navarro-Cía, M. Natrella, F. Dominec, J. C. Delagnes, P. Kužel, P. Mounaix, C. Graham, C. C. Renaud, A. J. Seeds, and O. Mitrofanov, Appl. Phys. Lett. **103**, 221103 (2013).
[27] F. D'Angelo, Z. Mics, M. Bonn, and D. Turchinovich, Opt. Express **22**, 12475 (2014).